Hindawi Publishing Corporation
Journal of Nanomaterials
Volume 2012, Article ID 425028, 5 pages
doi:10.1155/2012/425028

Research Article

Effect of Titanium Substitution on Magnetic Properties and Microstructure of Nanocrystalline Monophase Nd-Fe-B Magnets

Wang Cong,[1] Guo ZhiMeng,[1] Sui YanLi,[2] Bao XiaoQian,[2] and Chen ZhiAn[3]

[1] *Department of Materials Engineering, University of Science and Technology Beijing, Beijing 100083, China*
[2] *State Key Laboratory for Advanced Metals and Materials, University of Science and Technology Beijing, Beijing 100083, China*
[3] *Beijing Zhong Ke San Huan Hi-Tech Co., Ltd., Beijing 100190, China*

Correspondence should be addressed to Sui YanLi, yls@ustb.edu.cn

Received 1 March 2012; Revised 1 April 2012; Accepted 9 April 2012

Academic Editor: Ovidiu Crisan

$Nd_{12.3}Fe_{81.7-x}Ti_xB_{6.0}$ ($x = 0.5$–3.0) ribbons have been prepared by rapid quenching and subsequent annealing treatment. Effect of Ti substitution and annealing treatment on the microstructure, magnetic properties, and crystallization behavior of the ribbons was systematically investigated by the methods of differential scanning calorimeter (DSC), X-ray diffraction (XRD), transmission electron microscopy (TEM), and vibrating sample magnetometer (VSM). It is found that Ti addition may increase the crystallization temperature and stabilize the amorphous phase. Ti element inhibits the grain growth during crystallization process and finally refines the microstructure. The exchange coupling interactions and magnetic properties of the ribbons increase with increasing x from 0.5 to 1 and then decrease with further increasing $x \geq 1.5$. Optimum magnetic properties with $(BH)_{max} = 151.6\,kJ/m^3$, $H_{ci} = 809.2\,kA/m$, $J_r = 1.02\,T$ are achieved in the $Nd_{12.3}Fe_{80.7}Ti_1B_{6.0}$ ribbons annealed at 600°C for 10 min.

1. Introduction

Nanocomposite Nd-Fe-B permanent magnets have attracted considerable attention as a probable new generation of permanent magnets because of their high remanence, high maximum energy product, and low cost [1, 2]. The presence of the soft phases such as α-Fe and Fe_3B increases the remanence but the coercive field is decreased, so that their application is limited [3]. The alloys with Nd content higher than 11 at %, that is, close to the stoichiometry composition of $Nd_2Fe_{14}B$ and usually believed to be single phase structure, are being studied to further improve coercivity. Since the discovery of the nanocrystalline Nd-Fe-B magnets, extensive efforts have been made to improve magnetic properties of $Nd_2Fe_{14}B$-based magnets [4–6]. However, the obtainable $(BH)_{max}$ is still significantly lower than that predicted by theory. This phenomenon can be practically attributed to the difference between practical microstructure and theoretical model, which is of fine mixture of aligned hard magnetic grains and two ferromagnetic phases suitably dispersed, crystallographically, coherent, and mutually coupled. Elements such as Zr and Nb have been found to improve overall hard magnetic properties effectively by refining the microstructure [7–10]. Chang et al. [11] have reported that Zr and Ti addition can modify phase constitution and refine the grain size of the Nd-Fe-Ti-Zr-B rod fabricated by direct casting method, and to lead to the enhancement of the magnetic properties of the rods. The effect of Ti&C addition on the phase composition, microstructure, magnetic properties, temperature characteristics, and corrosion behavior of rapid-quenched Nd-Fe-B alloy has been investigated [9, 10, 12]. The combined addition of Ti and other elements such as C and Zr has been discussed a lot. However, the report of the single addition of pure Ti to Nd-Fe-B alloy is seldom. In this work, we present our research about the crystallization behavior, microstructure, and magnetic properties of single-phase $Nd_{12.3}Fe_{81.7-x}Ti_xB_{6.0}$ ribbons.

2. Experimental

The ingots with nominal composition of $Nd_{12.3}Fe_{81.7-x}Ti_xB_{6.0}$ ($x = 0, 0.5, 1.0, 1.5, 2.0, 2.5, 3.0$) were prepared by arc melting pure constituent elements under high-purity Ar atmosphere. The ingots were remelted four

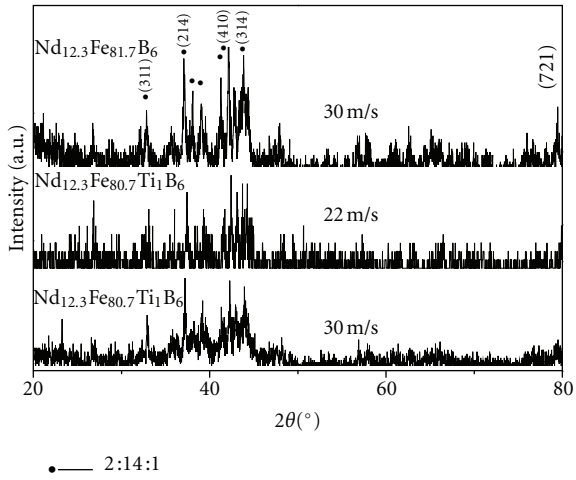

Figure 1: XRD patterns of $Nd_{12.3}Fe_{81.7-x}Ti_xB_{6.0}$ ribbons quenched at various wheel speeds.

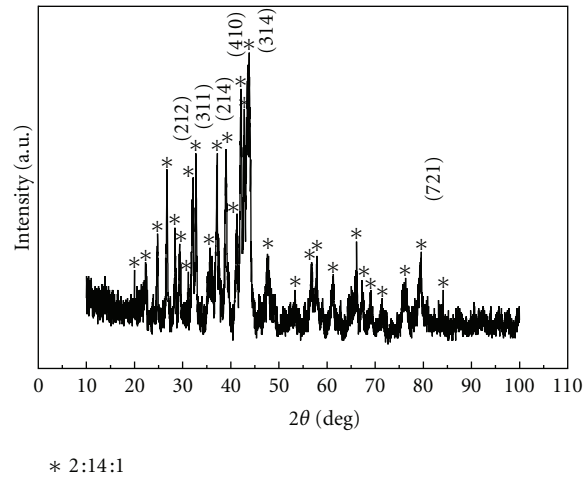

Figure 2: XRD patterns of as-cast $Nd_{12.3}Fe_{80.7}Ti_1B_6$ alloy annealed at 1050°C for 10 h.

times to ensure homogeneity. Ribbons with a width of 2–4 mm and thickness of 30–50 μm were obtained by ejecting the molten alloys from a quartz tube with an orifice diameter about 0.6 mm onto a copper wheel at a surface speed (Vs) of 22 m/s. The melt spun ribbons were then sealed in a quartz tube under a vacuum of 4×10^{-3} Pa and annealed at 550–800°C for 10 min to crystallize and develop desired fine nanoscale microstructure. Thermal analysis of the ribbons was carried out using NETZSCHSTA449 differential scanning calorimeter at a heating rate of 10°C/min to determine the crystallization temperature. Phases' analysis of the samples was characterized by D/max-rB X-ray diffractometer (Cu $K\alpha$ radiation). The microstructure of the ribbons was performed using with H-800 transmission electron microscopy (TEM). The thin foils for TEM observation were made by Ar-ion beam polishing. Hysteresis loops of the ribbons were measured using an LDJ 9600 vibrating sample magnetometer (VSM) with an applied field of up to 2 T (1600 kA/m). The length direction of the ribbons was parallel to the applied field in order to minimize the demagnetization effect. Wohlfarth's remanence analysis was employed to determine the strength of exchange-coupling interactions of the materials obtained.

3. Results and Discussion

3.1. Phase Analysis. Figure 1 shows XRD patterns of the as-spun $Nd_{12.3}Fe_{81.7-x}Ti_xB_{6.0}$ ($x = 0$, $x = 1$) ribbons with Vs of 22 m/s and 30 m/s. It can be seen that the ribbons are composed of amorphous phase and some $Nd_2Fe_{14}B$ phase, and the quantity and the relative intensity of diffraction peak for 2 : 14 : 1 decreases with increasing Vs from 22 m/s to 30 m/s and the addition Ti element, suggesting that the amount of 2 : 14 : 1 phase decreases and amorphous phase increases with increasing Vs and Ti content. The ribbons with $x = 0$ melt-spun by 30 m/s consist of hard magnetic 2 : 14 : 1 phase and some amorphous phase. The XRD patterns of the ribbons with $x = 1.0$ melt-spun by 20 m/s and 30 m/s present primarily amorphous phase. This indicates that Ti addition improves significantly the amorphization tendency of $Nd_{12.3}Fe_{81.7-x}Ti_xB_{6.0}$ alloys. Figure 2 shows XRD patterns of as-cast $Nd_{12.3}Fe_{80.7}Ti_1B_6$ alloy annealed at 1050°C for 10 h. It can be seen that amorphous phase transforms completely to 2 : 14 : 1 phase.

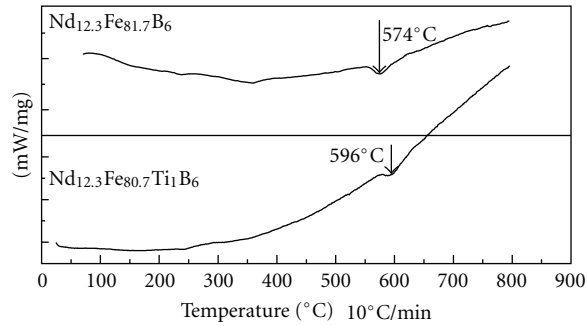

Figure 3: DSC curves of as-spun $Nd_{12.3}Fe_{81.7-x}Ti_xB_{6.0}$ ribbons at 30 m/s.

3.2. Effect of Ti on Crystallization Process and Microstructure. Figure 3 shows the differential scanning calorimetry (DSC) curves of the melt-spun $Nd_{12.3}Fe_{81.7-x}Ti_xB_{6.0}$ ribbons at a heating rate of 10 K/min from room temperature to 1073 K. The ribbons with $x = 0$ and 1 show one exothermic peak corresponding to transformation from amorphous to 2 : 14 : 1 structure. Compared to the ribbon with $x = 0$, the crystallization temperature peak T_p for the ribbon with $x = 1$ increases by approximately 20 K, indicating that Ti element enhances the thermal stability of amorphous phase in Nd-Fe-B alloy. Enrichment of Ti atoms along grain boundary stabilizes amorphous phase in the melt-spun and annealing process of the ribbons, which is believed to be a main reason that thermal stability is enhanced by Ti addition in the studied nanocrystalline $Nd_{12.3}Fe_{81.7}B_6$ magnets.

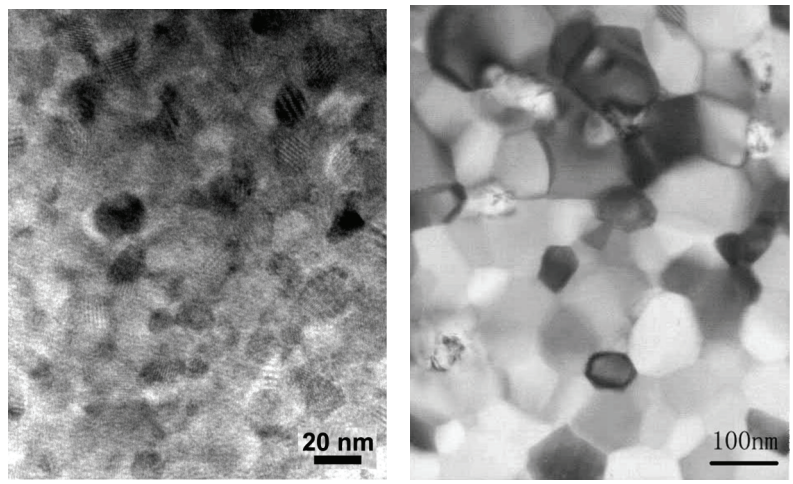

(a) (b)

FIGURE 4: TEM images of $Nd_{12.3}Fe_{80.7}Ti_1B_6$ (a) and $Nd_{12.3}Fe_{81.7}B_6$ (b) ribbons annealed at 600°C for 10 min.

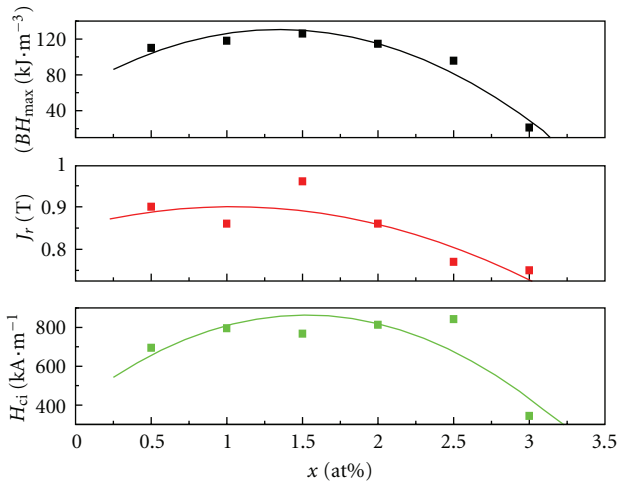

FIGURE 5: Variation of the J_r, H_{ci} and $(BH)_{max}$ with Ti content of as-spun $Nd_{12.3}Fe_{81.7-x}Ti_xB_{6.0}$ ribbons.

Figure 4 shows TEM bright field micrographs of (a) $Nd_{12.3}Fe_{80.7}Ti_1B_6$ and (b) $Nd_{12.3}Fe_{81.7}B_6$ ribbons annealed at 600°C for 10 min. The $Nd_{12.3}Fe_{81.7}B_6$ alloy shows an average grain size of around 80 nm and the grain size distribution is nonuniform. Large grains up to about 260 nm are present in the microstructure of the sample, which decreases exchange coupling interactions between neighbor grains. The average grain size is estimated to be 25 to 35 nm for the $Nd_{12.3}Fe_{80.7}Ti_1B_6$ alloy and the grains become more uniformly distributed. Thus, it can be concluded that the addition of a small amount of Ti to the ternary alloy is effective for reducing the grain size of the magnets, which enhances the coercive field and remanence. So the best magnetic property with $(BH)_{max} = 151.6\,kJ/m^3$ is obtained for the sample.

3.3. Effect of Ti Content on Magnetic Properties of Ribbons. The J_r, H_{ci}, and $(BH)_{max}$ of the $Nd_{12.3}Fe_{81.7-x}Ti_xB_{6.0}$ melt-spun ribbons by 22 m/s are shown in Figure 5. It is clear that the magnetic properties of melt-spun ribbons increase first with increasing Ti content, reaching the maximum value at $x = 1.5$, and then decrease with further increasing Ti content. The sample with $x = 3.0$ shows a very low coercivity and remanence.

The intrinsic coercivity H_{ci}, remanence polarization J_r, and maximum energy product $(BH)_{max}$ of the melt-spun ribbons are relatively low, which can be ascribed to incomplete crystallization of the ribbons, as evidenced by the superposition of broad peaks of amorphous precursor alloy and the characteristic of 2 : 14 : 1 peaks shown in Figure 1. In order to achieve the best magnetic properties for each alloy, a thermal treatment was employed individually to quenched ribbons to induce a fine grain structure crystallizing from the amorphous state. Figure 6 summarizes the effect of annealing temperature T_a and Ti content x on H_{ci}, J_r, and $(BH)_{max}$ of $Nd_{12.3}Fe_{81.7-x}Ti_xB_{6.0}$ ribbons. It can be seen that H_{ci}, J_r, and $(BH)_{max}$ increase first with increasing T_a and Ti content x, until reaching the maximum values, then decrease with further increasing T_a and Ti content x. Optimum magnetic properties with $(BH)_{max} = 151.6\,kJ/m^3$, $H_{ci} = 809.2\,kA/m$, $J_r = 1.02\,T$ are achieved by annealing the melt-spun ribbons with $x = 1.0$ at 600°C for 10 min, which are much higher than the magnetic properties of $Nd_6Pr_1Fe_{80}B_{13}$ ribbons with Ti&C addition reported by Ohkubo et al. [13].

Table 1 shows the variation of the optimum J_r/J_s, J_r, H_{ci}, and $(BH)_{max}$ with Ti content of the $Nd_{12.3}Fe_{81.7-x}Ti_xB_{6.0}$ ($x = 0.5$–3.0) ribbons. It can be seen that Ti addition significantly affects the magnetic properties of the samples. The J_r/J_s, J_r, H_{ci}, and $(BH)_{max}$ of optimally processed $Nd_{12.3}Fe_{81.7-x}Ti_xB_{6.0}$ ribbons initially increase with increasing Ti content from $x = 0.5$ to 1.0, but all of them decrease with further increasing Ti content. The J_r and H_{ci} increase from 0.79 T and 616.1 kA/m for the sample with $x = 0.5$ to 1.02 T and 809.2 kA/m for the sample with $x = 1.0$, respectively. The $(BH)_{max}$ of the 1.0 at.% Ti-doped sample increases from $76.2\,kJ/m^3$ to $151.6\,kJ/m^3$. Ti elements are benefit to refine grain sizes and enhance exchange coupling

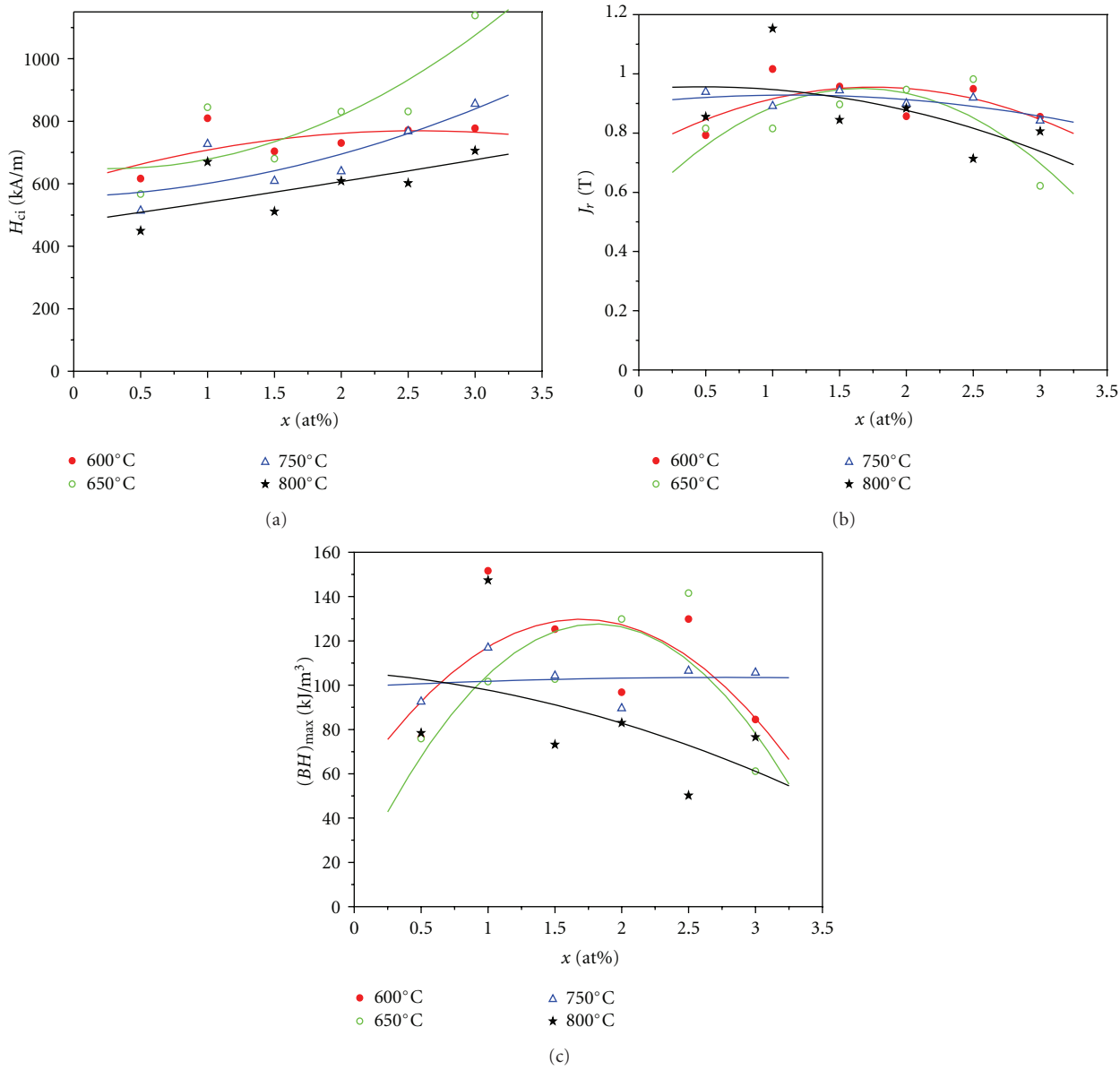

Figure 6: Magnetic properties of $Nd_{12.3}Fe_{81.7-x}Ti_xB_{6.0}$ ribbons annealed at various temperatures for 10 min.

Table 1: Magnetic properties of $Nd_{12.3}Fe_{81.7-x}Ti_xB_6$ ($x = 0.5, 1.0, 2.0, 3.0$) ribbons annealed at 600°C for 10 min.

x	$(BH)_{max}$ (kJ/m^3)	H_{ci} (kA/m)	J_r (T)	J_r/J_s
0.5	76.2	616.1	0.79	0.73
1.0	151.6	809.2	1.02	0.74
2.0	96.7	730.2	0.86	0.71
3.0	84.5	777.2	0.85	0.67

interactions between the neighbor grains. But the strength of exchange coupling interactions in the ribbons is determined by two opposite factors: (1) grain refinement and (2) magnetic dilution and grain isolation especially at higher Ti content.

3.4. Effect of Ti on Exchange Coupling. The exchange coupling interaction is often evaluated using δM plots, which can be defined as $m_d(H)$-(1-2 $m_r(H)$); where m_d is demagnetization remanence and m_r is isothermal magnetization remanence [14]. Both of these values are normalized by the saturation remanence. According to Wohlfarth's analysis, higher positive δM peaks indicate stronger exchange coupling interactions. Figure 7 shows the δM plots with respect to the applied magnetic field of the $Nd_{12.3}Fe_{81.7-x}Ti_xB_{6.0}$ annealed ribbons, respectively. The positive peak in the δM plots suggests the existence of exchange coupling interaction between $Nd_2Fe_{14}B$ and $Nd_2Fe_{14}B$ phases. It can be seen that the strength of exchange coupling interaction is significantly enhanced at a dilute Ti-substitution (1.0 at.% Ti) and then weakened when Ti content is further increased. This trend

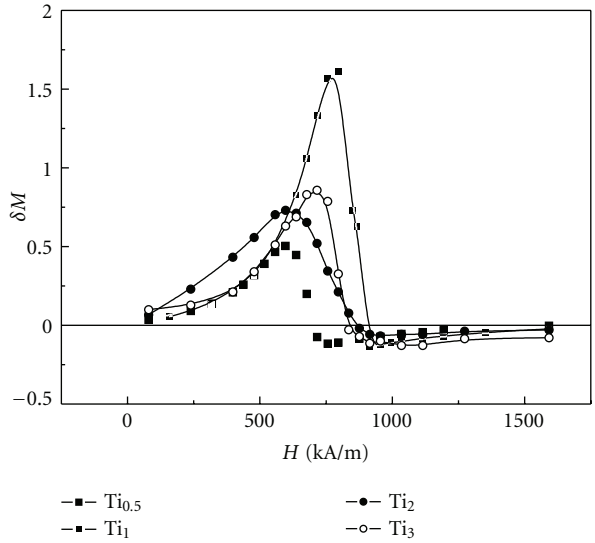

FIGURE 7: The $\delta M(H)$ curves of $Nd_{12.3}Fe_{81.7-x}Ti_xB_6$ ($x = 0.5, 1.0, 2.0, 3.0$) ribbons annealed at 600°C for 10 min.

agrees well with the variation of magnetic properties with Ti content previously shown in Figure 6. Hence, the changes in magnetic properties of the samples on increasing Ti content may mainly arise from the variation of the exchange-coupling interaction in the samples. Meanwhile, it is worth noting that the decrease of saturation magnetization with increasing Ti content also contributes to the reduction of J_r and $(BH)_{max}$, in the samples with higher Ti substitution.

4. Conclusion

The effect of Ti addition and annealing treatment on the magnetic properties and microstructure of nanocrystalline $Nd_{12.3}Fe_{81.7-x}Ti_xB_{6.0}$ ($x = 0.5$–3.0) alloys has been systematically investigated. The remanence polarization J_r, intrinsic coercivity H_{ci}, and maximum energy product $(BH)_{max}$ of optimally processed $Nd_{12.3}Fe_{81.7-x}Ti_xB_{6.0}$ ribbons increased first with an increase in Ti content, reached the maximum values at $x = 1.0$, then decreased with further increasing Ti content. The excellent magnetic properties with $(BH)_{max} = 151.6\,kJ/m^3$, $H_{ci} = 809.2\,kA/m$, $J_r = 1.02\,T$ were obtained by annealing a melt-spun amorphous $Nd_{12.3}Fe_{80.7}Ti_{1.0}B_{6.0}$ alloy at 600°C for 10 min. The variation of magnetic properties with increasing Ti content can be attributed to both the variation of the exchange coupling interactions and the decrease in saturation magnetization in the ribbons.

Acknowledgment

This work has been supported by the National Natural Science Foundation of China under Grant no. 51174030.

References

[1] E. F. Kneller and R. Hawig, "The exchange-spring magnet: a new material principle for permanent magnets," *IEEE Transactions on Magnetics*, vol. 27, no. 4, pp. 3588–3600, 1991.

[2] T. Schrefl, R. Fischer, J. Fidler, and H. Kronmüller, "Two- and three-dimensional calculation of remanence enhancement of rare-earth based composite magnets," *Journal of Applied Physics*, vol. 76, no. 10, pp. 7053–7058, 1994.

[3] C. P. Yang, Z. L. Jiang, X. Y. Chen et al., "Microstructure and magnetic properties of two-phase nanocomposite $Nd_9Fe_{85.5}Nb_{1.0}B_{4.5-y}Cy$ (y = 0.5–4.5) magnets," *Journal of Alloys and Compounds*, vol. 316, no. 1-2, pp. 269–274, 2001.

[4] Z. W. Liu and H. A. Davies, "The practical limits for enhancing magnetic property combinations for bulk nanocrystalline NdFeB alloys through Pr, Co and Dy substitutions," *Journal of Magnetism and Magnetic Materials*, vol. 313, no. 2, pp. 337–341, 2007.

[5] R. Gholamipour, A. Beitollahi, V. K. Marghusian, and T. Ohkubo, "Cu effects on coercivity and microstructural features in nanocrystalline Nd-Fe-Co-B annealed melt-spun ribbons," *Physica B*, vol. 398, no. 1, pp. 51–54, 2007.

[6] X. H. Li, Z. S. Gao, W. Li, K. W. Zhang, J. W. Zhang, and X. Y. Zhang, "Study of the microstructure of α-Fe/$Nd_2Fe_{14}B$ nanocomposites prepared by electropulsing heating amorphous NdFeCoB," *Materials Letters*, vol. 59, no. 22, pp. 2782–2785, 2005.

[7] R. Zhang, Y. Liu, J. Ye, W. Yang, Y. Ma, and S. Gao, "Effect of Nb substitution on the temperature characteristics and microstructures of rapid-quenched NdFeB alloy," *Journal of Alloys and Compounds*, vol. 427, no. 1-2, pp. 78–81, 2007.

[8] C. Wang, M. Yan, and W. Y. Zhang, "Significant changes in the microstructure, phase transformation and magnetic properties of $(Nd,Pr)_2Fe_{14}B/\alpha$-Fe magnets induced by Nb and Zr additions," *Materials Science and Engineering B*, vol. 123, no. 1, pp. 80–83, 2005.

[9] A. D. Crisan, "Compositional studies and thermal analysis in amorphous and nanocrystalline FePtNbB melt spun ribbons," *Journal of Optoelectronics and Advanced Materials*, vol. 12, no. 2, pp. 250–256, 2010.

[10] M. Seqqat, M. Nogues, O. Crisan et al., "Magnetic properties of $Fe_{100-x}Sm_x$ thin films and $Fe_{80-x}Sm_xB_v$ thin films and ribbons," *Journal of Magnetism and Magnetic Materials*, vol. 157-158, pp. 225–226, 1996.

[11] H. W. Chang, C. H. Chiu, C. W. Chang, W. C. Chang, A. C. Sun, and Y. D. Yao, "Effect of Ti substitution on the magnetic properties, microstructure, and aftereffect of melt spun PrFeB nanocomposites," *Scripta Materialia*, vol. 55, no. 6, pp. 529–532, 2006.

[12] R. Zhang, Y. Liu, J. Li, S. Gao, and M. Tu, "Effect of Ti&C substitution on the magnetic properties and microstructures of rapidly-quenched NdFeB alloy," *Materials Characterization*, vol. 59, no. 5, pp. 642–646, 2008.

[13] T. Ohkubo, T. Miyoshi, S. Hirosawa, and K. Hono, "Effects of C and Ti additions on the microstructures of $Nd_9Fe_{77}B_{14}$ nanocomposite magnets," *Materials Science and Engineering A*, vol. 448–451, pp. 435–439, 2007.

[14] M. Nezakat, R. Gholamipour, A. Amadeh, A. Mohammadi, and T. Ohkubo, "Corrosion behavior of $Nd_{9.4}Pr_{0.6}Fe_{bal.}Co_6B_6Ga_{0.5}Ti_xC_x$ ($x = 0, 1.5, 3, 6$) nanocomposites annealed melt-spun ribbons," *Journal of Magnetism and Magnetic Materials*, vol. 321, no. 20, pp. 3391–3395, 2009.